# Photonic-Assisted RF Self-Interference Cancellation With Improved Spectrum Efficiency and Fiber Transmission Capability

Yang Chen, *Member, IEEE*, and Jianping Yao, *Fellow, OSA*

***Abstract*—An approach to photonic-assisted carrier-suppressed single-sideband radio-frequency (RF) self-interference cancellation with improved spectrum efficiency and fiber transmission capability is proposed for in-band full-duplex radio-over-fiber systems. The key to achieve RF self-interference cancellation is to generate two single-sideband signals with one having a received signal with the RF self-interference signal and the other having only the RF self-interference signal, which is implemented by using a dual-polarization binary phase-shift keying (DP-BPSK) modulator. By controlling the arrival time and power of the electrical signals applied to the DP-BPSK modulator, the RF self-interference can be fully cancelled, and only a carrier-suppressed single-sideband signal with modulation is obtained. In addition to self-interference cancellation, the received signal can be directly converted to an optical baseband signal, so that the spectrum efficiency is increased. An experiment is performed. The results show that a cancellation depth of around 40 dB for a single-frequency self-interference and around 22 dB for a 100-Mbaud QPSK modulated wideband self-interference is achieved.**

***Index Terms*—In-band full-duplex radio-over-fiber system, microwave photonics, optical fiber dispersion, self-interference cancellation.**

## I. Introduction

During the past few years, radio-over-fiber (ROF) techniques have been actively researched thanks to the advantages of wide bandwidth and low loss when delivery of radio signals over fibers [1]–[3]. Conventionally, a base station in a full-duplex ROF system receives uplink signals from mobile users in a frequency band, while simultaneously transmitting downlink signals in a different frequency band. A sufficiently large frequency gap between the transmitting and receiving signals makes the base station have no interferences.

On the other hand, the limited spectral resource and the ever-increasing demand for higher data rates have motivated new in-band full-duplex communications, in which the uplink and downlink signals are located in the same frequency band [4]. Self-interference between the transmitting and receiving channels is the main issue to be solved in an in-band full-duplex communications system, and also in an in-band full-duplex ROF system, because it cannot be simply eliminated using electrical filters. Great efforts have been made to find solutions to eliminate self-interference in the electrical domain using electronic circuits [5], [6]. However, due to the well-known electronic bottleneck, the electrical self-interference cancellation (SIC) methods are limited in operating frequency and bandwidth. To overcome the limitations encountered in the electrical domain, radio-frequency (RF) SIC is desirable to be implemented using photonic-assisted solutions, to take advantages, such as low loss, wide bandwidth and high operating frequency, offered by modern photonics [7]–[9].

One early approach to implement photonic-assisted RF SIC was to use two parallel Mach-Zehnder modulators (MZMs) operating at different optical wavelengths [10]–[12]. The MZMs were biased at two opposite quadrature transmission points (QTP), and self-interference was cancelled in the electrical domain after the two photocurrents generated from the two wavelengths are combined at a photodetector (PD). In [13], two parallel electro-absorption modulators (EAMs) were used in conjunction with a balanced photodetector (BPD) to realize photonic-assisted RF SIC, where the self-interference was cancelled after subtraction at the BPD. To further simplify the system structure, two electro-absorption modulated lasers (EMLs) [14], [15], or two directly modulated lasers [16] were used instead of a single laser and two EAMs in [13]. An integrated microwave photonic circuit for photonic-assisted RF SIC based on the same concept was also demonstrated [17]. In [18]–[20], similar structures based on two EMLs and a single-port PD were proposed, where the signal subtraction was realized by inversing the interference signal directly in the electrical domain in the transmitter, so that the BPD can be replaced by a single-port PD. In [21], [22], photonic-assisted RF SIC based on parallel polarization modulators were proposed. The methods mentioned above all have a structure with two separated optical paths. The

Manuscript received August 13, 2019; revised October 7, 2019; accepted October 12, 2019. Date of publication October 15, 2019; date of current version February 12, 2020. This work was supported in part by the Natural Sciences and Engineering Research Council of Canada, in part by the National Natural Science Foundation of China under Grant 61971193 and Grant 61601297, in part by the Open Fund of IPOC (BUPT), and in part by the Fundamental Research Funds for the Central Universities. *(Corresponding author: Yang Chen.)*

Y. Chen is with the Shanghai Key Laboratory of Multidimensional Information Processing, East China Normal University, Shanghai 200241, China, with the Microwave Photonics Research Laboratory, School of Electrical Engineering and Computer Science, University of Ottawa, Ottawa, ON K1N 6N5, Canada, and also with the Engineering Center of SHMEC for Space Information and GNSS, East China Normal University, Shanghai 200241, China (e-mail: ychen@ce.ecnu.edu.cn).

J. Yao is with the Microwave Photonics Research Laboratory, School of Electrical Engineering and Computer Science, University of Ottawa, Ottawa, ON K1N 6N5, Canada (e-mail: jpyao@uottawa.ca).

Color versions of one or more of the figures in this article are available online at http://ieeexplore.ieee.org.

Digital Object Identifier 10.1109/JLT.2019.2947619

paths lengths must be precisely matched to enable effective RF SIC. For long-term operations, the path lengths must be actively controlled. In [23], [24], photonic-assisted RF SIC using a single modulator was proposed, the path length match problem was solved.

Note that most of the available RF SIC approaches were achieved in the electrical domain after photodetection. One problem associated with the cancellation in the electrical domain is that self-interference is still included in the optical signals before photodetection. Since these approaches are only focused on the cancellation of the self-interference signal, they are applicable to user terminal scenarios, where the received signals are directly used or processed. However, in a base station of an in-band full-duplex ROF system, the received RF signal is converted to an optical signal and then transmitted to the central station via optical fibers. When fiber dispersion is introduced, the phase relationship between the optical sidebands will change, which will influence the effectiveness of RF SIC. When the frequency of the RF signal is low, the influence caused by fiber dispersion is small and can be ignored. However, when the frequency of the RF signal is high, for example, tens of GHz, fiber dispersion will significantly change the phase relationship between optical sidebands, which would result in poor cancelation of self-interference after photodetection. Another problem when the frequency of the RF signal is high is the power fading effect [25]. If the optical signal transmitted in the optical fiber is a double-sideband with carrier signal, severe power fading of the received signal in the central station may happen. Recently, we have demonstrated two approaches to simultaneously realize RF SIC in the optical domain and overcome the power fading effect introduced by optical fiber via frequency down-conversion or single-sideband modulation [26], [27], thus the two problems mentioned above were both solved. However, one possible problem in [26], [27] is that the optical signal is a carrier-suppressed double-sideband (CS-DSB) or a single-sideband signal with carrier, which occupies a very large frequency band, so the spectrum efficiency is low. In addition, a CS-DSB modulated signal for intermediate-frequency (IF) signal generation in [26] was still affected by fiber dispersion, although the effect was greatly reduced due to a lower signal frequency.

In this paper, we propose a new approach to achieve RF SIC with improved spectrum efficiency and fiber transmission capability for in-band full-duplex ROF systems. The key to achieve RF SIC is to generate two single-sideband signals with one having a received signal with the RF self-interference signal and the other having only the RF self-interference signal, which is implemented by using a dual-polarization binary phase-shift keying (DP-BPSK) modulator. The DP-BPSK modulator consists of two dual-drive Mach-Zehnder modulators (DD-MZMs), which are both biased as optical single-sideband modulators. By combining the optical signals from the two DP-MZMs, the self-interference on the optical sideband is directly cancelled in the optical domain, with optical carrier suppressed. Using this method, received signals in an ROF system can be directly converted to an optical baseband signal. Furthermore, a local oscillator (LO) signal can be added to make the system to be an electrical IF receiver. The proposed approach can overcome the poor cancelation of the self-interference and the power fading effect of the received signal caused by fiber dispersion. In addition, the structure of the system is simplified and the spectrum efficiency is greatly improved as compared with the approach reported in [26], [27].

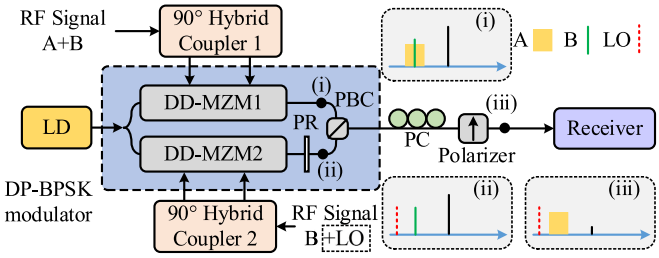


Fig. 1. Schematic diagram of the proposed carrier-suppressed single-sideband RF SIC system. LD, laser diode; DP-BPSK modulator, dual-polarization binary phase-shift keying modulator; DD-MZM, dual-drive Mach-Zehnder modulator; PBC, polarization beam combiner; PR, polarization rotator; PC, polarization controller.

## II. Principle

Fig. 1 shows the schematic diagram of the proposed carrier-suppressed single-sideband RF SIC system. A continuous-wave (CW) light wave generated from a laser diode (LD) is injected into a DP-BPSK modulator, which consists of a 3-dB optical coupler, two DD-MZMs, a 90° polarization rotator, and a polarization beam combiner (PBC). A corrupted signal (A + B) is applied to DD-MZM1 via the two RF ports through a 90° hybrid coupler, where A is a desired received signal, and B is a locally generated interference signal. The interference signal B is applied to DD-MZM2 as a reference signal via the two RF ports through another 90° hybrid coupler. Note that an LO signal can also be applied to DD-MZM2 if frequency down-conversion is needed. The optical signals with the polarization states aligned with the two orthogonal principal axes of the DP-BPSK modulator are sent via a polarization controller (PC) to a polarizer where the two signals are combined. The combined optical signals are detected in a receiver.

Assuming the desired RF signal is $V_1\cos(\omega_s t+\varphi_1)$, the interference signal at the same carrier frequency is $V_2\cos(\omega_s t+\varphi_2)$, where $V_1$ and $V_2$ are the amplitudes, $\varphi_1$ and $\varphi_2$ are the phase information of the desired and interference signals, respectively, and $\omega_s$ is the angular frequency of the RF signals, the optical signal from DD-MZM1, which is biased at the quadrature transmission point, can be expressed as

$$\begin{aligned} E_1(t) = \frac{1}{2}E_{in}(t)\Big\{&\exp\Big[jm_1\cos(\omega_s t+\varphi_1) \\ &+ jm_2\cos(\omega_s t+\varphi_2)+j\frac{\pi}{2}\Big], \\ &+\exp\left[jm_1\sin(\omega_s t+\varphi_1)\right. \\ &\left.+jm_2\sin(\omega_s t+\varphi_2)\right]\Big\} \end{aligned} \tag{1}$$

where $m_i=\pi V_i/V_\pi$ ($i$ = 1,2) is the modulation indices, $V_\pi$ is the switching voltage of the DP-BPSK modulator, and $E_{in}(t)$ is the input optical signal.

Using the Jacobi-Anger expansion and expanding (1) to the first order, we have

$$\begin{aligned} E_1(t) \approx \frac{1}{2}E_{in}(t)\,[&(1+j)\,J_0(m_1)\,J_0(m_2) \\ &+ (1-j)\,J_1(m_1)\,J_1(m_2)\cos(2\omega_s t+\varphi_1+\varphi_2) \\ &- (1+j)\,J_1(m_1)\,J_1(m_2)\cos(\varphi_1-\varphi_2) \\ &- 2J_0(m_1)\,J_1(m_2)\exp(-j\omega_s t-j\varphi_2) \\ &- 2J_0(m_2)\,J_1(m_1)\exp(-j\omega_s t-j\varphi_1)]\,, \end{aligned} \tag{2}$$

For DD-MZM2, we assume that the reference signal from the transmitter is $V_3\cos(\omega_s t+\varphi_2)$, and the LO signal is $V_{LO}\cos(\omega_{LO}t)$, where $V_3$ and $V_{LO}$ are the amplitudes of the reference signal and the LO signal, respectively, and $\omega_{LO}$ is the angular frequency of the LO signal. The optical signal at the output of DD-MZM2 can be expressed as

$$\begin{aligned} E_2(t) = \frac{1}{2}E_{in}(t)\Big\{&\exp\Big[jm_3\cos(\omega_s t+\varphi_2) \\ &+ jm_{LO}\cos(\omega_{LO}t)+j\frac{\pi}{2}\Big] \\ &+ \exp\left[jm_3\sin(\omega_s t+\varphi_2)+jm_{LO}\sin(\omega_{LO}t)\right]\Big\}\,, \end{aligned} \tag{3}$$

where $m_3=\pi V_3/V_\pi$ and $m_{LO}=\pi V_{LO}/V_\pi$ are the modulation indices. Again, using the Jacobi-Anger expansion and expanding (3) to the first order, we have

$$\begin{aligned} E_2(t) \approx \frac{1}{2}E_{in}(t)\,[&(1+j)\,J_0(m_3)\,J_0(m_{LO}) \\ &+ (1-j)\,J_1(m_3)\,J_1(m_{LO}) \\ &\times\cos(\omega_s t+\omega_{LO}t+\varphi_2) \\ &- (1+j)\,J_1(m_3)\,J_1(m_{LO}) \\ &\times\cos(\omega_s t-\omega_{LO}t+\varphi_2) \\ &- 2J_0(m_3)\,J_1(m_{LO})\exp(-j\omega_{LO}t) \\ &- 2J_0(m_{LO})\,J_1(m_3)\exp(-j\omega_s t-j\varphi_2)]\,. \end{aligned} \tag{4}$$

Since the two optical signals from the two DD-MZMs are aligned with two principal axes of the DP-BPSK modulator, respectively, the optical signal from the DP-BPSK modulator are applied to a polarizer via a PC with its principal axis oriented at an angle of 135° to one principle axis of the DP-BPSK modulator to combine the optical signals at the two orthogonal polarization directions with a $\pi$ phase shift. Therefore, the optical signal from the polarizer is given by

$$\begin{aligned} E_o(t) = \frac{\sqrt{2}}{4}E_{in}(t)\,\{&(1+j)\,J_0(m_1)\,J_0(m_2) \\ &- (1+j)\,J_0(m_3)\,J_0(m_{LO}) \\ &+ (1-j)\,J_1(m_1)\,J_1(m_2)\cos(2\omega_s t+\varphi_1+\varphi_2) \\ &- (1-j)\,J_1(m_3)\,J_1(m_{LO})\cos(\omega_s t+\omega_{LO}t+\varphi_2) \\ &- (1+j)\,J_1(m_1)\,J_1(m_2)\cos(\varphi_1-\varphi_2) \\ &+ (1+j)\,J_1(m_3)\,J_1(m_{LO})\cos(\omega_s t-\omega_{LO}t+\varphi_2) \\ &+ 2\left[J_0(m_{LO})\,J_1(m_3)-J_0(m_1)\,J_1(m_2)\right] \\ &\times\exp(-j\omega_s t-j\varphi_2) \\ &- 2J_0(m_2)\,J_1(m_1)\exp(-j\omega_s t-j\varphi_1) \\ &+ 2J_0(m_3)\,J_1(m_{LO})\exp(-j\omega_{LO}t)\}\,. \end{aligned} \tag{5}$$

Under small signal modulation condition ($m_1, m_2, m_3, m_{LO} << 1$), (5) can be further simplified as

$$\begin{aligned} E_o(t) \approx \frac{\sqrt{2}}{4}E_{in}(t)\,\{&-2J_0(m_2)\,J_1(m_1)\exp(-j\omega_s t-j\varphi_1) \\ &+ 2\left[J_0(m_{LO})\,J_1(m_3)-J_0(m_1)\,J_1(m_2)\right] \\ &\times\exp(-j\omega_s t-j\varphi_2) \\ &+ 2J_0(m_3)\,J_1(m_{LO})\exp(-j\omega_{LO}t)\}\,. \end{aligned} \tag{6}$$

As can be seen from (6), a first-order optical sideband of the RF signal carrying both the information from the desired signal and the interference signal, as well as a first-order optical sideband of the LO signal, is generated, in which the optical carrier is suppressed. In order to cancel the self-interference directly in the optical domain, the self-interference signal and the reference signal applied to the two DD-MZMs should have an equal arrival time, and the following condition should also be satisfied,

$$J_0(m_{LO})\,J_1(m_3) = J_0(m_1)\,J_1(m_2)\,, \tag{7}$$

which means the power of the signals should also be controlled. In fact, under small signal modulation condition, the relationship between the modulation indices can be relaxed to $m_2 = m_3$. Under these conditions, (6) can be simplified as

$$\begin{aligned} E_o(t) = \frac{\sqrt{2}}{4}E_{in}(t)\,[&-2J_0(m_2)\,J_1(m_1)\exp(-j\omega_s t-j\varphi_1) \\ &+ 2J_0(m_3)\,J_1(m_{LO})\exp(-j\omega_{LO}t)]\,. \end{aligned} \tag{8}$$

As can be seen, a first-order optical sideband carrying only the information of the desired signal and a first-order optical sideband of the LO signal are generated with the optical carrier fully suppressed and self-interference fully cancelled. Since the optical carrier is suppressed, the generated optical signal occupies a much small bandwidth as compared with the approaches in [26], [27], resulting in a much higher spectrum efficiency. After detecting the optical signal at the PD, the desired signal is generated at the IF band with the self-interference completely cancelled.

Under a special case, where the LO signal is disconnected from the system, i.e., $m_{LO}=0$, the optical signal shown in (8) is given by

$$E_o(t) = -\frac{\sqrt{2}}{2}E_{in}(t)\,J_0(m_2)\,J_1(m_1)\exp(-j\omega_s t-j\varphi_1)\,. \tag{9}$$

Equation (9) indicates that only a first-order optical sideband carrying the desired signal is generated with the optical carrier fully suppressed and the self-interference fully cancelled. Compared with the case that employs an LO signal, the received

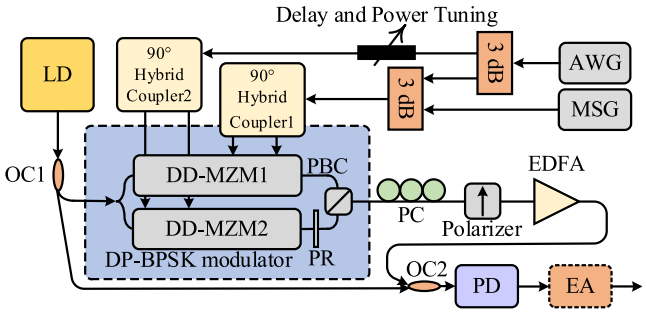


Fig. 2. Experimental setup of the proposed carrier-suppressed single-sideband RF SIC system. LD, laser diode; OC, optical coupler; DP-BPSK modulator; dual-polarization binary phase-shift keying modulator; PBC, polarization beam combiner; PR, polarization rotator; PC, polarization controller; EDFA, erbium-doped fiber amplifier; PD, photodetector; EA, electrical amplifier; MSG, microwave signal source; AWG, arbitrary waveform generator.

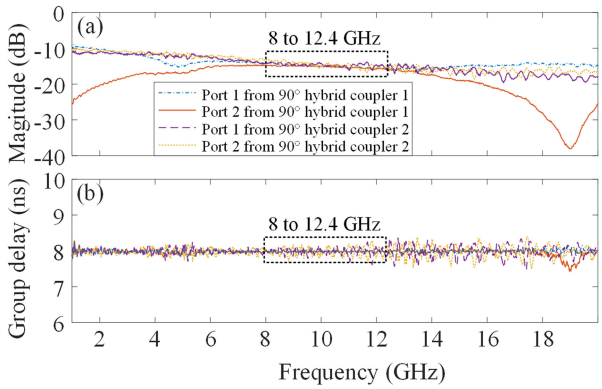


Fig. 3. Measured $S_{21}$ parameters of the four electrical paths from the AWG to the two DD-MZM. (a) Magnitude response and (b) group delay response.

signal is directly converted to an optical baseband signal, so that the spectrum efficiency is further increased and RF down-conversion in the system is no longer needed. It should be noticed that if the desired signal is a phase-modulated signal as shown in the deductions, an optical LO signal should be employed in the receiver to convert the phase-modulated signal to a signal in the IF band or in the baseband. However, it can be easily derived that when the modulated signal is an intensity-modulated signal, the optical baseband signal can be directly detected at a PD to recover the information.

## III. Experimental Results

Fig. 2 shows the experimental setup of the proposed carrier-suppressed single-sideband RF SIC system. A CW light wave from an LD (Anritsu MG9638A) is sent to a DP-BPSK modulator (Fujitsu FTM 7980EDA) through an optical coupler (OC1). The DP-BPSK modulator has a 3-dB bandwidth of about 20 GHz. The interference RF signal is generated from an arbitrary waveform generator (AWG, Keysight M8195A), which is split into two paths by a 3-dB electrical coupler and applied to the DP-BPSK modulator. Specifically, one output from the electrical coupler is sent to a 90° hybrid coupler with precise power and delay control, and the other output of the electrical coupler is combined with an desired RF signal from a microwave signal generator (MSG, Agilent E8254A) in a second 3-dB electrical coupler, and then sent to a second 90° hybrid coupler. The two outputs from each 90° hybrid coupler are applied to one of the two DD-MZMs in the DP-BPSK modulator. The optical signal from the DP-BPSK modulator is sent to a polarizer via a PC, and then amplified by an erbium-doped fiber amplifier (EDFA) and combined with an unmodulated optical carrier from the LD at another optical coupler (OC2), and then applied to a PD. Note that the unmodulated optical carrier is used to heterodyne with the carrier-suppressed single-sideband modulated signals to show the RF SIC performance in the electrical domain.

First, the system is adjusted to make the self-interference signal and the reference signal applied to the two DD-MZMs have the same arrival time and power. The $S_{21}$ parameters of the four electrical paths are measured by a vector network analyzer (VNA, Keysight N5224A), with the results shown in Fig. 3. The 3-dB bandwidth of the two 90° hybrid couplers are from 8 to 12.4 GHz and from 1 to 18 GHz, thus the operating bandwidth of the system is limited from 8 to 12.4 GHz. As shown in Fig. 3(a), the four magnitude responses of the four paths are very close over the whole bandwidth from 8 to 12.4 GHz with a maximum variation of less than 2 dB. Fig. 3(b) shows the group delays of the four paths, which all vary around 8 ns. By further adjusting the time delay and amplitude, the $S_{21}$ parameters of the four paths can be made very close in a small bandwidth, in which, the RF SIC can be implemented.

Then, the RF SIC is investigated in the optical domain. In the study, the desired RF signal is disconnected from the system. The power of the optical signal centered at 1553.275 nm from the LD is set at 8 dBm, and the power of the single-frequency self-interference RF signal is set at 20 dBm. The optical spectra from the two DD-MZMs and the polarizer with and without RF SIC are measured using an optical spectrum analyzer (OSA, Ando AQ6317B) and shown in Fig. 4, with the frequency of the self-interference signal tuned from 8 to 12.4 GHz.

As shown in Fig. 4, the optical signals from the two DD-MZMs have similar optical spectra, which both consist of an optical carrier and a first-order optical sideband. When the RF SIC is enabled without the desired RF signal, the optical carrier and the first-order optical sideband that have relatively high power from the DD-MZMs are both deeply suppressed. When one path of the interference signal is disconnected from the system, the suppressed first-order optical sideband reappears, whereas the optical carrier is still deeply suppressed. From the optical spectra shown in Fig. 4 with and without RF SIC, a self-interference cancellation depth of more than 44 dB is achieved.

Then, wideband RF SIC is also verified in the optical domain. Since the resolution bandwidth of the OSA is 0.015 nm, the wideband self-interference signal from the AWG is selected as a 5-Gbaud QPSK modulated RF signal with 1 V amplitude to have a better observation of the RF SIC by monitoring the optical spectrum. Fig. 5(a) and (b) shows the measured optical spectra when the frequency of the RF signal is set at 10.2 and 12.4 GHz, respectively. The two outputs from the two

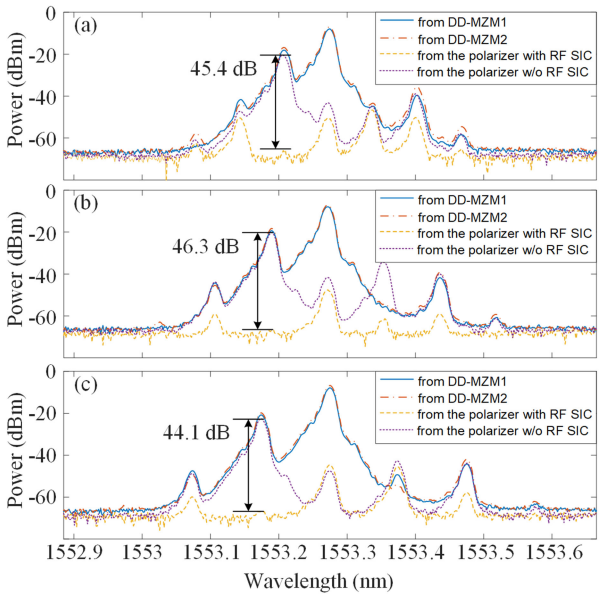


Fig. 4. Measured optical spectra with and without RF SIC when the central frequencies of the input single-frequency self-interference signals are (a) 8 GHz (b) 10.2 GHz, and (c) 12.4 GHz.

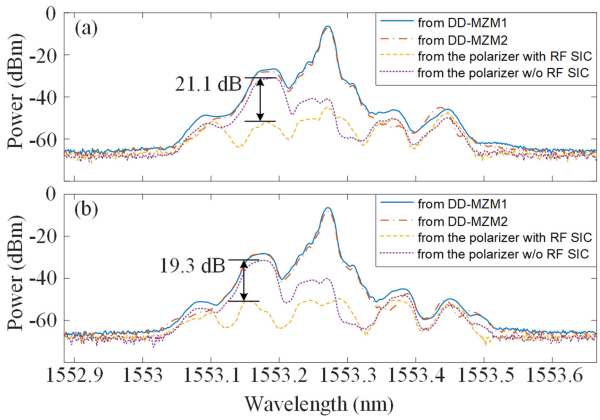


Fig. 5. Measured optical spectra with and without RF SIC when the central frequencies of the input wideband self-interference signals are (a) 10.2 GHz and (b) 12.4 GHz.

DD-MZMs have about the same optical spectra, both with an optical carrier and a first-order optical sideband. It should be noticed that the first-order optical sideband is modulated by the wideband self-interference signal, and the optical carrier is information free, due to the small signal modulation condition. When the RF SIC is enabled, the pure optical carrier and the data-modulated first-order optical sideband are both deeply suppressed. Furthermore, if one path of the wideband self-interference signal is disconnected from the system, the data-modulated first-order optical sideband reappears and the optical carrier is still suppressed. From the optical spectra shown in Fig. 5(a) and (b) with and without RF SIC, a self-interference cancellation depth of more than 19 dB is achieved. It is noticed that when the pure optical carrier is suppressed, a modulated spectral profile on it appears, which is the very weak modulation

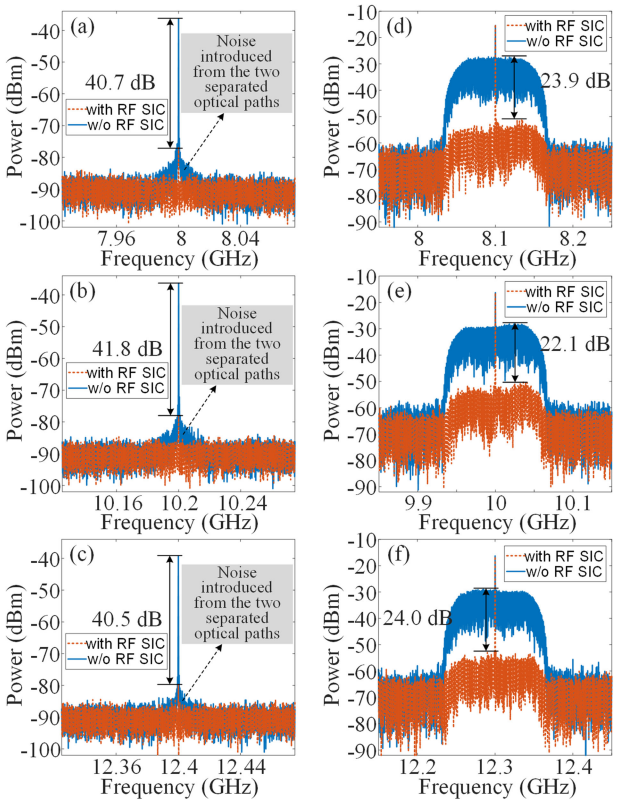


Fig. 6. Electrical spectra of the RF signal with and without single-frequency RF SIC when the central frequencies of the input signals are (a) 8 GHz, (b) 10.2 GHz, and (b) 12.4 GHz; electrical spectrum of the RF signal with and without wideband RF SIC when the central frequencies of the input signals are (d) 8.1 GHz, (e) 10 GHz, and (f) 12.3 GHz.

component on the optical carrier under small signal modulation condition.

In the above experiment, the desired RF signal is not applied to the system because it is difficult to distinguish it from the self-interference signal via the optical spectrum. However, if the desired RF signal is connected, the first-order optical sideband from DD-MZM1 contains both the self-interference and the desired RF signal, whereas the optical carrier remains almost unchanged due to the small signal modulation condition. The optical signal from DD-MZM2 remains unchanged. Therefore, after combing at the polarizer, it can be easily known that only a first-order optical sideband of the desired RF signal is generated, with the optical carrier suppressed.

Then, the RF SIC is demonstrated in the electrical domain after photodetection. The power of the optical and electrical signals is the same as that used in the demonstration of RF SIC in the optical domain. Since the generated optical signal after RF SIC is a carrier-suppressed single-sideband signal that cannot be directly detected in a PD, we use OC1 and OC2 to direct an optical carrier from the LD for converting the optical sideband to an RF signal. Fig. 6(a)–(c) shows the single-frequency RF SIC, where the frequencies of the self-interference signal are 8, 10.2 and 12.4 GHz, respectively. When the RF SIC is enabled, the single-frequency self-interference is more than 40 dB suppressed in these three cases. The three RF signals without RF

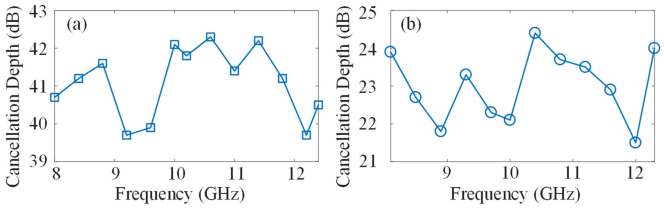


Fig. 7. Cancellation depth for a (a) single-frequency self-interference signal and (b) wideband self-interference (200-Mbps QPSK) signal.

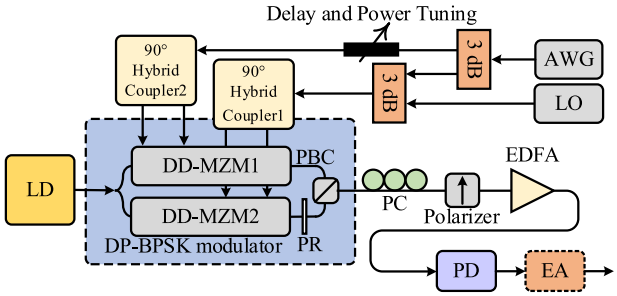


Fig. 8. Experimental setup of the proposed carrier-suppressed single-sideband RF SIC system when an LO signal is introduced.

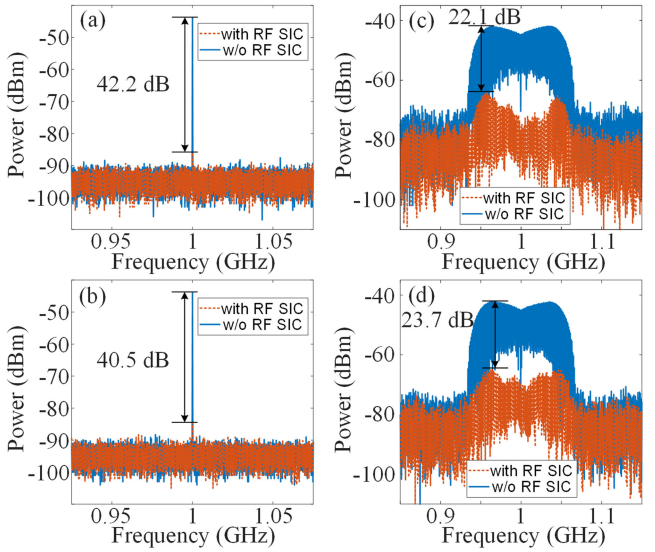


Fig. 9. Electrical spectrum of the down-converted IF signal with and without single-frequency RF SIC when the central frequencies of the input signals are (a) 10.2 GHz and (b) 12.4 GHz; electrical spectrum of the RF signal with and without wideband RF SIC when the central frequencies of the input signals are (c) 10.2 GHz and (d) 12.3 GHz.

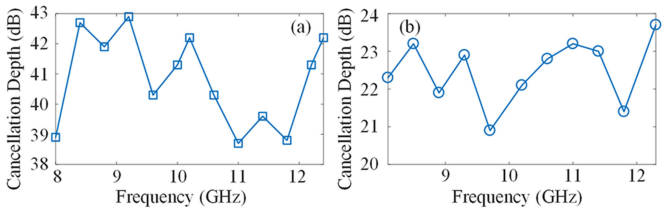


Fig. 10. Cancellation depth of a (a) single-frequency self-interference signal and (b) wideband self-interference (200-Mbps QPSK) signal.

SIC do not show very good noise performance. This is caused by the beating between the optical carrier and the first-order optical sideband from two physically separated optical paths.

The wideband RF SIC in the electrical domain is also demonstrated. In the experiment, the desired RF signal is a pure RF signal, whereas the self-interference signal is a 100-Mbaud QPSK modulated signal with its frequency tuning from 8.1 to 12.3 GHz. Since the self-interference signal from the AWG is only 1 V, the generated electrical signal at the output of the PD has very low power. Therefore, a low-noise electrical amplifier with 45-dB gain from 8 to 18 GHz is used to amplify the RF signal from the PD. Fig. 6(d)–(f) shows the wideband RF SIC, with the central frequencies of the self-interference signal tuned from 8.1 to 12.3 GHz. When the RF SIC is disabled, the desired pure RF signal is mixed with the wideband self-interference. In contrast, if the RF SIC is enabled, the wideband self-interference is cancelled with a cancellation depth of more than 22 dB, whereas the desired pure RF signal does not have significant power degradation.

Fig. 7 shows the cancellation depth of the proposed system versus the central frequency of the RF signal. For the single-frequency RF SIC, the cancellation depths are around 41 dB, whereas those for the wideband RF SIC are around 23 dB.

Then, the performance of the system with an LO signal that is used to perform frequency down-conversion is also verified. An LO signal is combined with the reference signal, and then applied to DD-MZM2. In the experiment, the frequency of the LO signal is set to 1 GHz lower than that of the RF signal. The structure of the experimental setup is shown in Fig. 8.

Fig. 9(a) and (b) shows the electrical spectra of the down-converted 1-GHz IF signals for the single-frequency RF SIC, where cancellation depths of 42.2 dB and 40.5 dB are achieved for RF signals at 10.2 and 12.4 GHz, respectively. Fig. 9(c) and (d) shows the electrical spectra of the down-converted 1-GHz IF signals with and without the wideband RF SIC. It should be noticed that no desired RF signal is applied to the modulator, thus, no discrete frequency component at the center of the spectra is observed as compared with those shown in Fig. 6. The cancellation depths for the 10.2 and 12.3 GHz wideband self-interference are 22.1 dB and 23.7 dB, respectively.

The cancellation depth of the system with an LO signal is also verified and shown in Fig. 10. For the single-frequency RF SIC, the cancellation depths vary around 40 dB. For the wideband RF SIC, the cancellation depths are around 22 dB.

Since the single-sideband carrier-suppressed operation is implemented, only a first-order optical sideband of the desired RF signal is generated if no LO signal is applied. When the LO signal is applied, an IF signal from the PD is generated by beating the first-order optical sidebands of the LO signal and the desired RF signal. Different from the results shown in [26], where the IF signal is generated by combing two beating products from the lower first-order optical sidebands and the higher first-order optical sidebands, the IF signal generated here is only generated

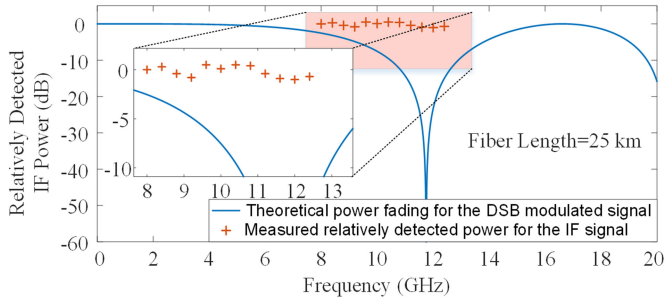


Fig. 11. Theoretical power fading for the DSB modulated signal and the measured relatively detected power for the IF signal generated in this article, when the length of the optical fiber is 25 km.

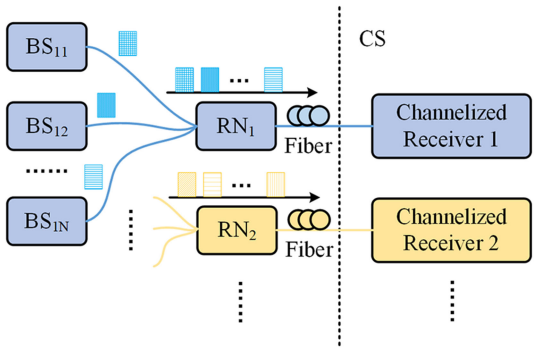


Fig. 12. Schematic diagram of the application of the proposed RF SIC technique in an ROF system. BS, base station; RN, remote node; CS, central station.

by one beating product either from the lower first-order optical sidebands or the higher first-order optical sidebands. Although the power fading effect in [26] is very small, the work here has further improvement with no power fading effect. Since the power fading effect for 1-GHz IF transmission is very small, we only compare the power fading effect of the proposed system with that of the DSB-modulated signal, with the results shown in Fig. 11. When the length of the optical fiber is 25 km, serious power fading effect is observed as the solid curve for the DSB-modulated signals. In the experiment, we measure the power of the 1-GHz IF signal with the frequency of the RF signal tuned from 8 to 12.4 GHz, which is shown as cross line in Fig. 11. The optical power is normalized to remove the influence of the frequency response of the system. As can be seen from Fig. 11, the power of the received 1-GHz IF signal remains nearly unchanged in the whole frequency tuning range, which proves the effectiveness of the approach in the elimination of the power fading effect.

In the experimental demonstration, we only verified the performance of the system in a frequency range from 8 to 12.4 GHz, which is limited by the operating bandwidth of one of the 90° hybrid couplers. In fact, the operating frequency range of the system can be further increased by using 90° hybrid couplers with wider bandwidths.

In practical applications, the received signals in a base station are combined at a remote node and then transmitted to the central station. If no LO signal is applied, the received signal in a base station is a baseband-modulated optical signal with no self-interference. Therefore, different baseband optical signals from different base stations can be multiplexed in a remote note, as shown in Fig. 12, and then transmitted to the central station, where a channelized receiver [28] can be used to channelize and demodulate the desired received signals from different base stations. Without electrical or optical filtering, the technique can not only realize RF SIC in the optical domain to make it suitable for fiber transmission, but also convert the RF signal modulation in an ROF system to an optical baseband modulation, which greatly improves the spectrum efficiency, reduces system complexity, and makes it possible to combine with the photonic-based channelized receiver.

## IV. Conclusion

We have theoretically and experimentally investigated a photonic-assisted carrier-suppressed single-sideband RF SIC system with improved spectrum efficiency and fiber transmission capability for in in-band full-duplex ROF systems based on a DP-BPSK modulator. The key contribution of the work was that the self-interference in the RF band was cancelled in the optical domain with the desired RF signal simultaneously converted to the baseband or the IF band with carrier-suppressed single-sideband operation, thus, the spectrum efficiency of the system was greatly improved. In addition, the cancellation of the self-interference in the optical domain and the carrier-suppressed single-sideband operation made the system perfectly immune to the fiber dispersion, so the proposed system was very suitable for signal transmission from a base station to the central station in an in-band full-duplex ROF system after the RF SIC is realized in the base station. An experiment was carried out. RF SIC from 8 to 12.4 GHz was demonstrated in both single frequency and wideband. The cancellation depth was around 40 dB for the single-frequency self-interference, and that for the 100-Mbaud QPSK modulated wideband self-interference was around 22 dB. The influence on the power of the transmitted signal was also evaluated and the results showed no significant power degradation.

## References

[1] T. Kuri, H. Toda, J. Olmos, and K. Kitayam, "Reconfigurable dense wavelength-division-multiplexing millimeter-waveband radio-over-fiber access system technologies," *J. Lightw. Technol.*, vol. 28, no. 16, pp. 2247–2257, Aug. 2010.

[2] N. Gomes *et al.*, "Radio-over-fiber transport for the support of wireless broadband services," *J. Opt. Netw.*, vol. 8, no. 2, pp. 156–178, Feb. 2009.

[3] C. Lim, A. Nirmalathas, M. Bakaul, K. L. Lee, D. Novak, and R. Waterhouse, "Mitigation strategy for transmission impairments in millimeterwave radio-over-fiber networks," *J. Opt. Netw.*, vol. 8, no. 2, pp. 201–214, Feb. 2009.

[4] Y. Dong, H. Yüksel, and A. Molnar, "A wideband highly integrated and widely tunable transceiver for in-band full-duplex communication," *IEEE J. Solid-State Circuits*, vol. 50, no. 5, pp. 1189–1202, May 2015.

[5] M. Duarte, C. Dick, and A. Sabharwal, "Experiment-driven characterization of full-duplex wireless systems," *IEEE Trans. Wireless Commun.*, vol. 11, no. 12, pp. 4296–4307, Dec. 2012.

[6] S. Hong, J. Brand, J. Choi, and M. Jain, "Applications of self-interference cancellation in 5G and beyond," *IEEE Commun. Mag.*, vol. 52, no. 2, pp. 114–121, Feb. 2014.

[7] J. Capmany and D. Novak, "Microwave photonics combines two worlds," *Nature Photon.*, vol. 1, no. 6, pp. 319–330, Jun. 2007.
[8] J. Yao, "Microwave photonics," *J. Lightw. Technol.*, vol. 27, no. 3, pp. 314–335, Feb. 2009.
[9] D. Marpaung, C. Roeloffzen, R. Heideman, A. Leinse, S. Sales, and J. Capmany, "Integrated microwave photonics," *Laser Photon. Rev.*, vol. 7, no. 4, pp. 506–538, Jul. 2013.
[10] J. Suarez, K. Kravtsov, and P. Prucnal, "Incoherent method of optical interference cancellation for radio-frequency communications," *IEEE J. Quantum Electron.*, vol. 45, no. 4, pp. 402–408, Apr. 2009.
[11] J. Suarez and P. Prucnal, "Instantaneous bandwidth of counter-phase optical interference cancellation for RF communications," *IEEE Microw. Wireless Compon. Lett.*, vol. 21, no. 9, pp. 507–509, Sep. 2011.
[12] J. Chang and P. Prucnal, "A novel analog photonic method for broadband multipath interference cancellation," *IEEE Microw. Wireless Compon. Lett.*, vol. 23, no. 7, pp. 377–379, Jul. 2013.
[13] M. Change, M. Fok, A. Hofmaier, and P. Prucnal, "Optical analog self-interference cancellation using electro-absorption modulators," *IEEE Microw. Wireless Compon. Lett.*, vol. 23, no. 2, pp. 99–101, Feb. 2013.
[14] Y. Zhang, L. Li, S. Xiao, M. Bi, Y. Yu, and W. Hu, "Wideband over-the-air RF self-interference cancellation by an EML-based optical system with baseband predistortion," *IEEE Photon. J.*, vol. 9, no. 5, Oct. 2017, Art. no. 5503009.
[15] Y. Zhang *et al.*, "Experimental study of wideband in-band full-duplex communication based on optical self-interference cancellation," *Opt. Exp.*, vol. 24, no. 26, pp. 30139–30148, Dec. 2016.
[16] S. Zhang, S. Xiao, Y. Zhang, H. Feng, L. Zhang, and Z. Zhou, "Directly modulated laser-based optical radio frequency self-interference cancellation system," *Opt. Eng.*, vol. 55, no. 2, Feb. 2016, Art. no. 026116.
[17] M. Chang, E. Blow, M. Lu, J. Sun, and P. Prucnal, "RF characterization of an integrated microwave photonic circuit for self-interference cancellation," *IEEE Trans. Microw. Theory Techn.*, vol. 66, no. 1, pp. 596–605, Jan. 2018.
[18] J. Sun, M. Chang, and P. Prucnal, "Demonstration of over-the-air RF self-interference cancellation using an optical system," *IEEE Photon. Technol. Lett.*, vol. 29, no. 4, pp. 397–400, Feb. 2017.
[19] Q. Zhou, H. Feng, G. Scott, and M. Fok, "Wideband co-site interference cancellation based on hybrid electrical and optical techniques," *Opt. Lett.*, vol. 39, no. 22, pp. 6537–6540, Nov. 2014.
[20] Q. Zhou, J. Ge, and M. Fok, "Fast dynamic in-band RF self-interference cancellation for enabling efficient spectral usage," in *Proc. Opt. Fiber Commun. Conf. Exhib.*, Los Angeles, CA, USA, 2017, Paper W4B.5.
[21] M. Huang, D. Zhu, and S. Pan, "Optical RF interference cancellation based on a dual-parallel polarization modulator," in *Proc. Asia Commun. Photon. Conf.*, Shanghai, China, 2014, Paper ATh1F.6.
[22] W. Zhou, P. Xiang, Z. Niu, M. Wang, and S. Pan, "Wideband optical multipath interference cancellation based on a dispersive element," *IEEE Photon. Technol. Lett.*, vol. 28, no. 8, pp. 849–851, Apr. 2016.
[23] Y. Zhang, S. Xiao, H. Feng, L. Zhang, Z. Zhou, and W. Hu, "Self-interference cancellation using dual-drive Mach–Zehnder modulator for in-band full duplex radio-over-fiber," *Opt. Express*, vol. 23, no. 26, pp. 33205–33213, Dec. 2015.
[24] X. Han, B. Huo, Y. Shao, and M. Zhao, "Optical RF self-interference cancellation by using an integrated dual-parallel MZM," *IEEE Photon. J.*, vol. 9, no. 2, Apr. 2017, Art. no. 5501308.
[25] Y. Chen, A. Wen, L. Shang, and Y. Wang, "A full-duplex radio-over-fiber link with 12-tupling mm-wave generation and wavelength reuse for upstream signal." *Opt. Laser Technol.*, vol. 43, no. 7, pp. 1167–1171, Oct. 2011.
[26] Y. Chen and S. Pan, "Simultaneous wideband radio-frequency self-interference cancellation and frequency downconversion for in-band full-duplex radio-over-fiber systems," *Opt. Lett.*, vol. 43, no. 13, pp. 3124–3127, Jul. 2018.
[27] B. Weng, M. Chang, and Y. Chen, "Radio-frequency self-interference cancellation using a dual-drive Mach–Zehnder modulator and a fiber Bragg grating," *Opt. Eng.*, vol. 57, no. 8, Aug. 2018, Art. no. 08310.
[28] W. Hao *et al.*, "Chirped-pulse-based broadband RF channelization implemented by a mode-locked laser and dispersion," *Opt. Lett.*, vol. 42, no. 24, pp. 5234–5237, Dec. 2017.

**Yang Chen** (S'12–M'17) received the B.E. degree in telecommunications engineering, in 2009, and the Ph.D. degree in communication and information systems, in 2015, from Xidian University, Xi'an, China.

In 2017, he joined the School of Communication and Electronic Engineering, East China Normal University, Shanghai, China, where he is currently a Research Professor. From 2012 to 2014, he was a joint-training Ph.D. student with the Microwave Photonics Research Laboratory, School of Electrical Engineering and Computer Science, University of Ottawa, Ottawa, ON, Canada. His current research interests include microwave photonics, optoelectronic oscillators, radio-over-fiber techniques, and optical communications.

**Jianping Yao** (M'99–SM'01–F'12) received the Ph.D. degree in electrical engineering from the Université de Toulon et du Var, Toulon, France, in December 1997. He is a Distinguished University Professor and a University Research Chair with the School of Electrical Engineering and Computer Science, University of Ottawa, Ottawa, ON, Canada. From 1998 to 2001, he was with the School of Electrical and Electronic Engineering, Nanyang Technological University, Singapore, as an Assistant Professor. In December 2001, he joined the School of Electrical Engineering and Computer Science, University of Ottawa, as an Assistant Professor, where he was promoted to an Associate Professor in May 2003, and to a Full Professor in May 2006. He was appointed as the University Research Chair in Microwave Photonics in 2007. In June 2016, he was conferred the title of Distinguished University Professor of the University of Ottawa. From July 2007 to June 2010 and July 2013 to June 2016, he was the Director of the Ottawa-Carleton Institute for Electrical and Computer Engineering. He has authored or coauthored more than 560 research papers including more than 330 papers in peer-reviewed journals and more than 230 papers in conference proceedings.

Prof. Yao is the Editor-in-Chief for the IEEE PHOTONICS TECHNOLOGY LETTERS, a Topical Editor for *Optics Letters*, an Associate Editor for *Science Bulletin*, a Steering Committee Member for the IEEE JOURNAL OF LIGHTWAVE TECHNOLOGY, and an Advisory Editorial Board member for *Optics Communications*. He was a Guest Editor of a Focus Issue on Microwave Photonics in *Optics Express* in 2013, a Lead-Editor of a Feature Issue on Microwave Photonics in *Photonics Research* in 2014, and a Guest Editor of a special issue on Microwave Photonics in the IEEE JOURNAL OF LIGHTWAVE TECHNOLOGY in 2018. He currently serves as the Chair of the IEEE Photonics Ottawa Chapter, and is the Technical Committee Chair of IEEE MTT-3 Microwave Photonics. He was a member of the European Research Council Consolidator Grant Panel in 2016, the Qualitative Evaluation Panel in 2017, and a member of the National Science Foundation Career Awards Panel in 2016. He has also served as a Chair of a number of international conferences, symposia, and workshops, including the Vice Technical Program Committee (TPC), Chair of the 2007 IEEE Topical Meeting on Microwave Photonics, a TPC Co-chair of the 2009 and 2010 Asia-Pacific Microwave Photonics Conference, a TPC Chair of the high-speed and broadband wireless technologies subcommittee of the IEEE Radio Wireless Symposium 2009–2012, a TPC Chair of the microwave photonics subcommittee of the IEEE Photonics Society Annual Meeting 2009, a TPC Chair of the 2010 IEEE Topical Meeting on Microwave Photonics, a General Co-Chair of the 2011 IEEE Topical Meeting on Microwave Photonics, a TPC Cochair of the 2014 IEEE Topical Meetings on Microwave Photonics, and a General Co-Chair of the 2015 and 2017 IEEE Topical Meeting on Microwave Photonics. He has also served as a committee member for a number of international conferences, such as IPC, OFC, BGPP, and MWP. He was the recipient of the 2005 International Creative Research Award of the University of Ottawa, the 2007 George S. Glinski Award for Excellence in Research, and the Natural Sciences and Engineering Research Council of Canada Discovery Accelerator Supplements Award in 2008. He was selected to receive an inaugural OSA Outstanding Reviewer Award in 2012 and was one of the top ten reviewers of IEEE/OSA Journal of Lightwave Technology 2015–2016. He was an IEEE MTT-S Distinguished Microwave Lecturer for 2013–2015. He was the recipient of the Award for Excellence in Research 2017–2018 of the University of Ottawa. He is a registered Professional Engineer of Ontario. He is a Fellow of the Optical Society of America, the Canadian Academy of Engineering, and the Royal Society of Canada.